Dynamic stall control over an airfoil by NS-DBD actuation*

He-Sen Yang(杨鹤森)[1], Guang-Yin Zhao(赵光银)[2,†], Hua Liang(梁华)[1,‡], and Biao Wei(魏彪)[1]

[1] *Science and Technology on Plasma Dynamics Laboratory, Air Force Engineering University, Xi'an* 710038, *China*
[2] *State Key Laboratory of Aerodynamics, China Aerodynamics Research and Development Center, Mianyang* 621000, *China*

(Received 3 July 2020; revised manuscript received 6 August 2020; accepted manuscript online 25 August 2020)

The wind tunnel test was conducted with an NACA 0012 airfoil to explore the flow control effects on airfoil dynamic stall by NS-DBD plasma actuation. Firstly, light and deep dynamic stall states were set, based on the static stall characteristics of airfoil at a Reynolds number of 5.8×10^5. Then, the flow control effect of NS-DBD on dynamic stall was studied and the influence law of three typical reduced frequencies ($k = 0.05$, $k = 0.05$, and $k = 0.15$) was examined at various dimensionless actuation frequencies ($F^+ = 1$, $F^+ = 2$, and $F^+ = 3$). For both light and deep dynamic stall states, NS-DBD had almost no effect on upstroke. However, the lift coefficients on downstroke were increased significantly and the flow control effect at $F^+ = 1$ is the best. The flow control effect of the light stall state is more obvious than that of deep stall state under the same actuation conditions. For the same stall state, with the reduced frequency increasing, the control effect became worse. Based on the in being principles of flow separation control by NS-DBD, the mechanism of dynamic stall control was discussed and the influence of reduced frequency on the dynamic flow control was analyzed. Different from the static airfoil flow separation control, the separated angle of leading-edge shear layer for the airfoil in dynamic stall state is larger and flow control with dynamic oscillation is more difficult. The separated angle is closely related to the effective angle of attack, so the effect of dynamic stall control is greatly dependent on the history of angles of attack.

Keywords: flow control, dynamic stall, dielectric barrier discharge (DBD), nanosecond pulse, reduced frequency

PACS: 52.30.–q, 47.85.Ld, 47.20.Ib, 47.32.Ff **DOI:** 10.1088/1674-1056/abb227

1. Introduction

Dynamic stall is a kind of intense unsteady and nonlinear delayed flow phenomenon caused by a large range of flow separation over the wings or blades when the angle of attack changes periodically or dramatically with time.[1] This phenomenon is commonly found in the retreating blades of helicopter,[2–4] fast pitch maneuvering fighters,[5] wind turbine blades,[6] and rotating surging compressors,[7] which leads to unsteady flutter and vibratory loads.

The unsteady loads generated by dynamic stall will directly affect the mechanical properties of various aircrafts, especially helicopter, and the maneuverability, gas-elastic stability, noise and propulsion will also be damaged. Therefore, it is significant to use flow control methods to improve unsteady aerodynamic characteristics of dynamic stall airfoil and reduce or even avoid the risk and harm brought by dynamic stall.

Although great progress has been made in the understanding of unsteady flow separation control in recent years,[8–10] dynamic stall is still one of the major problems in aerodynamics. With the analysis of flow field evolution, the stall accompanied with flutter and a sharp drop in lift is found to be caused by the generation and appearance of dynamic stall vortex (DSV).[11] Thus, the major purpose of dynamic stall control is to explore the effective methods to control DSV.[12] Figure 1 shows the flow field of airfoil dynamic stall within a pitch period, the formation and movement of DSV can be seen clearly.

Previous researches have tried many passive and active methods in this purpose.[14,15] Passive methods work by making geometric modifications to the airfoil, which may result in noise and vibration at off-design circumstances.[16] Conventional active methods can provide benefit over a broader operating range compared to passive devices. But at the same time, this requires a prohibitive amount of momentum injection, which is not worth the cost.[17,18] Therefore, new cost-effective method is urgently needed.

In the last decades, plasma actuation has become one of the most popular active flow control methods due to its advantages of simple structure, rapid response, and wide frequency band. In terms of flow separation control, dielectric barrier discharge (DBD) has been extensively studied. Typical DBD actuation method includes DBD driven by altering current high voltage (AC-DBD) and DBD driven by nanosecond pulses (NS-DBD).[19] It is confirmed that AC-DBD mainly produces the momentum effect for flow separation control, and NS-DBD mainly relies on its fast heating effect.[20]

In recent years, NS-DBD has shown great potential in flow separation control of steady flows over a wide range of

*Project supported by the National Natural Science Foundation of China (Grant No. 11802341) and the Open Fund from State Key Laboratory of Aerodynamics of China (Grant No. SKLA20180207).

†Corresponding author. E-mail: zym19860615@163.com
‡Corresponding author. E-mail: lianghua82702@126.com

Mach numbers ($Ma \leq 0.75$) and Reynolds numbers ($10^4 < Re < 2 \times 10^6$)[21] that are consistent with retreating blade flows. However, dynamic stall control based on plasma actuation has not been widely studied. In 2004, the first research on AC-DBD controlling an oscillating NACA 0015 airfoil appeared. Subsequently, some studies using AC-DBD for dynamic stall control have emerged, which demonstrates that dynamic stall could be controlled by AC-DBD. Since 2018, few relevant researches based on NS-DBD have emerged. Frankhouser M has found that NS-DBD actuation could improve stall state and promote the early recovery of wing's upper surface pressure.[22] Starikovskiy A has confirmed that NS-DBD can alleviate the dynamic stall for a Reynolds number of 4.5×10^5 and reduced frequency of 0.02.[23] Mo Samimy has carried out experimental research at combinations of different Reynolds numbers ($Re = 1.67 \times 10^5$, $Re = 3 \times 10^5$, and $Re = 5 \times 10^5$) and reduced frequencies ($k = 0.025$–0.075), find that NS-DBD results in earlier reattachment.[23,24]

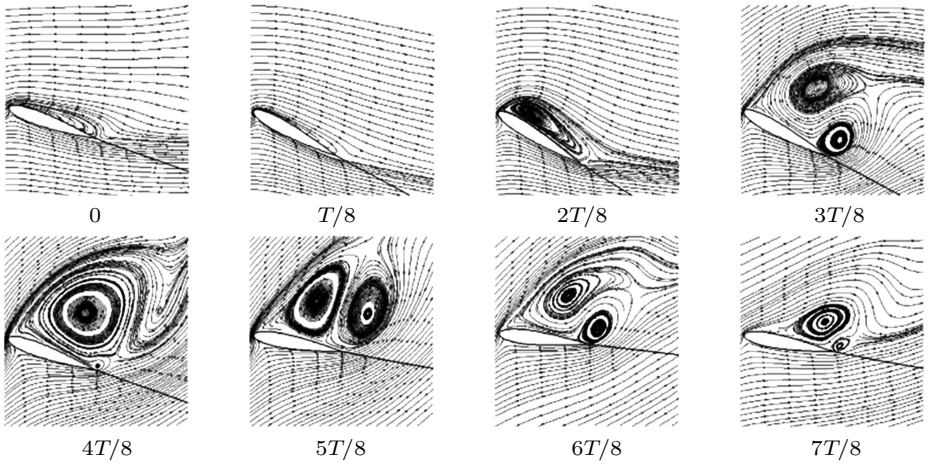

Fig. 1. Flow field of airfoil dynamic stall within a pitch period.[13]

However, the reduced frequency and Reynolds number in previous studies is still comparatively small. Typically, the largest reduced frequency attempt in previous studies is $k = 0.075$,[24] but for the real helicopter application, the range of reduced frequency for rotor is $k = 0.05$–0.15.[25] Hence, dynamic stall control at larger reduced frequencies and higher Reynolds numbers is indispensable. What is more, previous studies usually focus on a certain stall state, the effect of NS-DBD dynamic stall flow control for different stall states on an airfoil has not been given enough attention. Above all, the research on dynamic stall flow control mechanism is still preliminary.

In this paper, the wind tunnel tests of dynamic stall control over an NACA 0012 airfoil by NS-DBD actuation at a Reynolds number of 5.8×10^5 were conducted. The flow control effect at different reduced frequencies ($k = 0.05$, $k = 0.05$, and $k = 0.15$) and various dimensionless actuation frequencies ($F^+ = 1$, $F^+ = 2$, and $F^+ = 3$) was tested and analyzed under light and deep dynamic stall conditions through direct aerodynamic force measurement. Based on the experimental results, the flow control mechanisms were discussed preliminarily.

2. Experimental set-up and preliminary test

Experiments were performed in the recirculating wind tunnel of Nanjing University of Aeronautics and Astronautics. The wind tunnel has an open test section measuring 5 m (length)×3.4 m (width)×2.4 m (height), which can produce freestream velocities up to 50 m/s with the axial turbulence intensity on the order of 1.44%. An NACA 0012 airfoil with a 300-mm-chord and a 0.75-m-wingspan was employed. Airfoil installation in the wind tunnel is shown in Fig. 2.

The airfoil is connected to its oscillation driving device by a spar located at the quarter-chord line. The power of the device comes from a DC motor. As shown in Fig. 3, a rocker arm connected to the airfoil is driven by an eccentric wheel to realize the oscillation of the airfoil. An angle senor is fixed at a coaxial beam to the airfoil.

The motion of the airfoil $\alpha(t)$ is described by three parameters: mean angle of attack α_0, motion amplitude α_m, and reduced frequency k ($k = \pi fc/U_\infty$ where f is the oscillation frequency of the airfoil, c is the airfoil chord, and U_∞ is the freestream velocity). The motion of the airfoil is defined as a sinusoidal curve, $\alpha(t) = \alpha_0 + \alpha_m \times \sin(\omega t)$, where t is time in seconds and $\omega = 2\pi f$ is the angular frequency. The mean angle of attack and motion amplitude can be adjusted by the eccentric distance and the length of the rocker arm. The oscillation frequency can be set by altering the parameters of frequency converter connected to the DC motor.

To measure the aerodynamic forces of the airfoil, a six-component strain balance is installed under the airfoil oscillation drive device. The strain gauge directly measures the

forces and moments on the airfoil so the aerodynamic forces acting along the entire span are quantified. The data are acquired by an NI PXI 4220 capture card, whose acquisition frequency is adjustable. In this paper, it was set to 3000 Hz. Before the experiments, the balance was calibrated and its acquisition system's repeatability was validated.

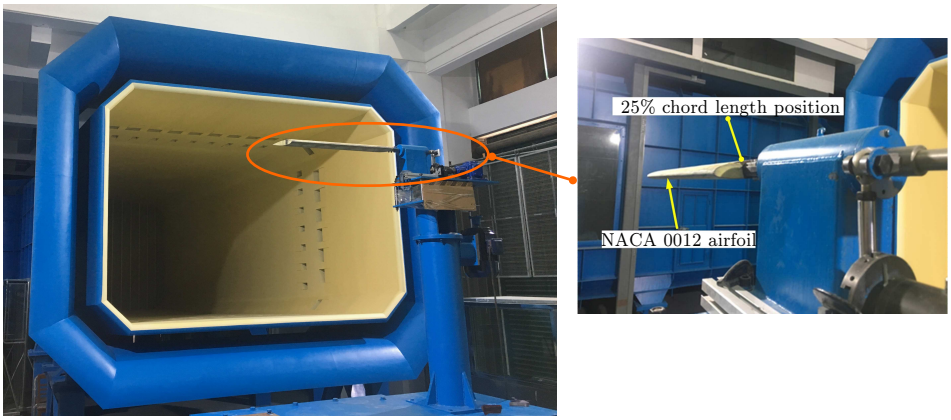

Fig. 2. Airfoil installation and experimental layout in wind tunnel.

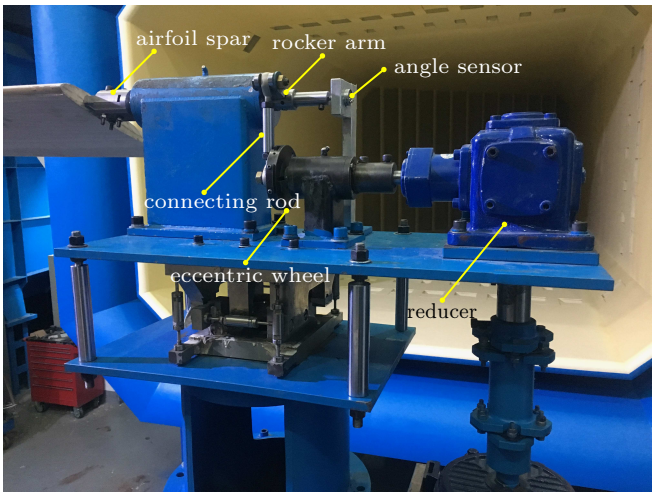

Fig. 3. Airfoil oscillation drive device.

The plasma actuation system consists of the DBD actuator, the high-voltage power supply, and the electrical parameter measuring system. The actuator consists of the exposed electrode, covered electrode and dielectric layer and is powered by a nanosecond pulse power supply. The electrodes, made of copper tape (0.027-mm thickness), are separated by a Kapton dielectric layer (0.18-mm thickness). Dissimilarly, the width of the exposed electrode is 5 mm and that of the encapsulated electrode is 10 mm. The actuator was placed on the leading edge of the airfoil with the electrode junction at $x/c = 0$ (shown in Fig. 4), covering the entire span of the airfoil. The plasma region is on the suction side. The electrical parameters of plasma discharge are measured by a DPO4104 digital oscilloscope, a P6015A high voltage probe, and a P6022 AC current probe.

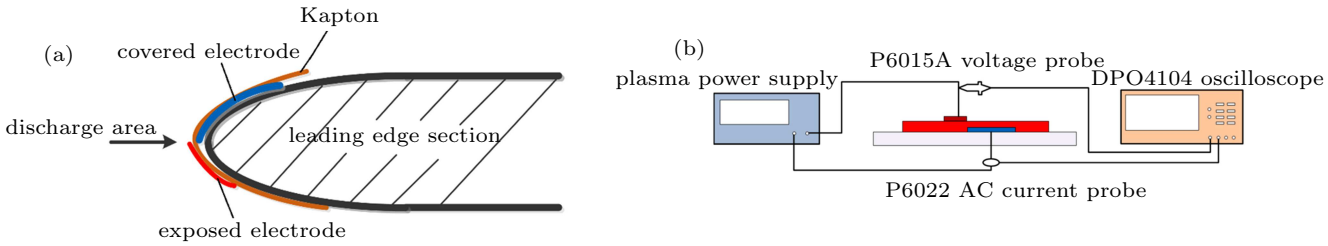

Fig. 4. Deployment of actuator at the leading edge of airfoil and electrical parameter measurement: (a) deployment of actuator. (b) system of electrical parameter measurement.

The nanosecond pulse power supply used in the experiment has a nominal power of 200 W and can generate voltage pulses as high as 20 kV. The repetition frequency of the voltage pulse is continuously adjustable from 1 Hz to 20 kHz. The actuator is driven by a nanosecond pulse to produce strong impulse perturbations at the leading edge. The leading edge is the receptivity region of the shear layer instabilities, which is the location of maximum sensitivity to perturbations on airfoil.[12] Before the wind tunnel test, ground characteristics of the plasma actuation were tested based on a 0.75-m-length actuator in still air. Results show that the discharge energy can be instantaneously converted into heat, causing an instantaneous pressure rise and inducing a shock wave, as shown in Fig. 5.

The shock wave is caused by the thermal effect caused by the instantaneous breakdown of air by discharge.[19] Through calculation, the propagation velocity of the shock wave is 335 m/s, which is approximately equal to the speed of sound.

On the one hand, NS-DBD heats up local air to convert electric energy into heat energy, which is released instantaneously. The gas expands under heat, causing a sudden rise in local temperature and generating shock waves. The speed of the shock wave is relatively fast, and it has a relatively large instantaneous thrust. On the other hand, the heated air carries a lot of heat and it lasts for a long time. With the evolution of time, it diffuses in all directions, and the disturbance area is large, resulting in a local high temperature region, which mainly exerts a thermal effect on the convection field.

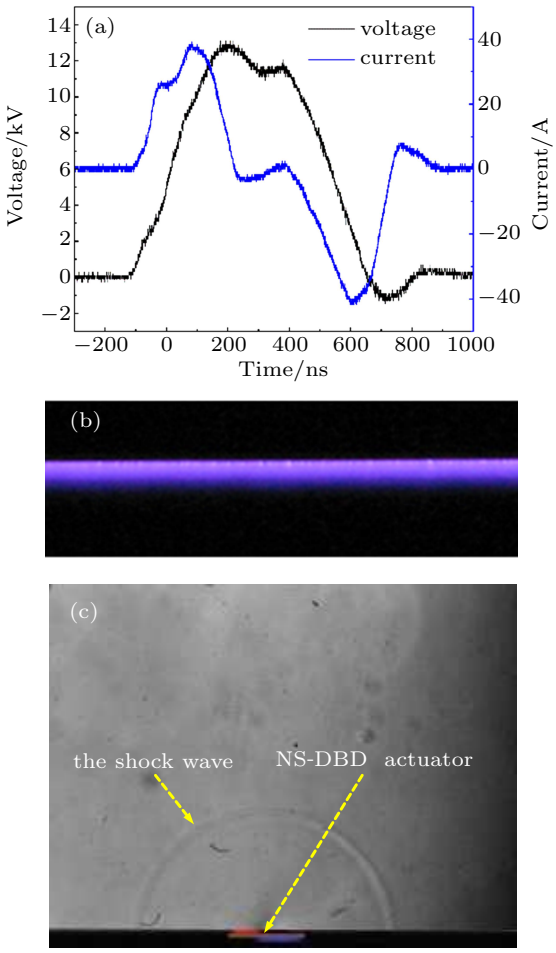

Fig. 5. Characteristics of NS-DBD in still air: (a) voltage and current curves of NS-DBD ($V_{p-p} = 13$ kV), (b) discharge image of NS-DBD, and (c) shock wave induced by NS-DBD experimental results.

3. Experimental results

3.1. Static stall characteristics

Firstly, the static experiment was carried out to explore the effect of the physical presence of the actuator (when not in use) and verify the control capability of NS-DBD on the static aerodynamic coefficients with a static temperature of 25 °C. The experimental conditions correspond to a freestream velocity $U_\infty = 30$ m/s, a temperature of 25 °C, a gas density $\rho = 1.185$ kg/m^3, a dynamic viscosity $\mu = 1.835 \times 10^5$, and a Reynolds number $Re = 5.8 \times 10^5$. As shown in Fig. 6, a slight difference in the lift coefficient with and without the presence of plasma actuator can be observed, indicating the minimal impact of the actuator when not in use. The baseline stall angle of the airfoil is 17°, and lift is significantly improved when plasma on, with the stall angle delayed to 21°.

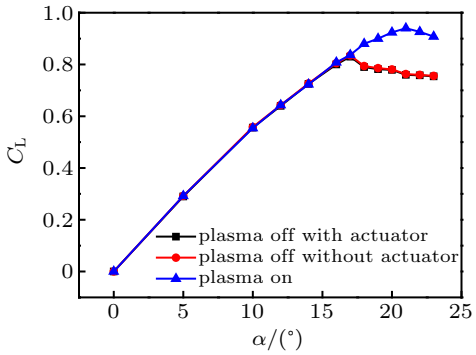

Fig. 6. Static experimental lift coefficient C_L under different airfoil's profile states.

According to the static results, two dynamic stall states (light stall state and deep stall state) were designed, as shown in Table 1. Here, the reduced frequency is a non-dimensional parameter to describe the flow instability over the airfoil. Since the range of reduced frequency for helicopter retreating blades is generally from 0.05 to 0.15, three typical conditions ($k = 0.05$, $k = 0.1$, and $k = 0.15$) were selected under light and deep stall states. The flow control effects and related control laws for k were analyzed under the set stall states.

Table 1. List of dynamic stall states.

Stall state	$\alpha_0/(^\circ)$	$\alpha_m/(^\circ)$	Range of $\alpha/(^\circ)$	k
Light stall	13.1	7.9	5.2–21	0.05, 0.1, 0.15
Deep stall	14.85	9.45	5.4–24.3	0.05, 0.1, 0.15

3.2. Flow control of light stall state

The airfoil's motion profile was $\alpha = 13.1 + 7.9^\circ \times \sin(\omega t)$ under light dynamic stall, with $\omega = 2kU_\infty/c$. With the freestream velocity of $U_\infty = 30$ m/s, dynamic stall control was conducted under various reduced frequencies ($k = 0.05$, $k = 0.1$, and $k = 0.15$) and dimensionless actuation frequencies ($F^+ = 1$, $F^+ = 2$, and $F^+ = 3$). The dimensionless frequency is defined as $F^+ = f_0 c/U_\infty$, where f_0 is the frequency of the high-voltage pulses. Three dimensionless frequencies were arranged to ensure that NS-DBD could be efficient in each reduced frequency state. The peak-to-peak voltage was fixed at $V_{p-p} = 13$ kV with plasma on.

Figure 7 shows the baseline lift coefficient for various reduced frequencies. As the airfoil starts pitching up, the boundary layer is attached and the lift coefficient increases steadily with α. When α exceeds the static (critical) stall angle, the lift continues to increase. At this moment, the vorticity at the leading edge accumulates and the dynamic stall vortex begins to form. The dynamic stall vortex formation is accompanied

by counter-rotating vortices on the airfoil's surface. These vortices travel upstream, pushed by the dynamic stall vortex, resulting in the detachment of the dynamic stall vortex.[26] After the dynamic stall vortex has convected, the airfoil is fully stalled with a sharp drop in the lift coefficient. Then, the boundary layer gradually attaches on downstroke and lift coefficient slowly rises up. Finally, the boundary layer is fully attached at small α, and the lift coefficient also returns to the level of upstroke.

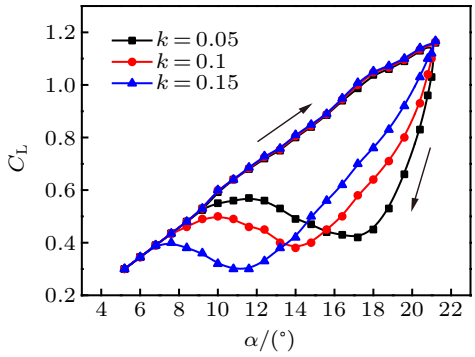

Fig. 7. Baseline for various reduced frequencies of light dynamic stall.

As the reduced frequency increasing, the peak lift coefficient is almost unchanged but the flow separation is reduced while a delayed flow reattachment is also observed. Larger reduced frequency means greater flow instability over the airfoil. Chandrasekhara[27] conjectured that this is due to the increasing pitch rate enabling the boundary layer to withstand higher levels of adverse pressure gradient. After characterizing the baseline flow, various dimensionless actuation frequencies were used in the flow control appilacations to determine the NS-DBD's flow control capabilities at three typical reduced frequencies.

3.2.1. Flow control effects at $k = 0.05$

Figure 8 shows the lift coefficients at $Re = 5.8 \times 10^5$, $k = 0.05$ and various dimensionless actuation frequencies. All the states of actuation have little effect on upstroke and the lift coefficient at maximum α is not promoted. At the beginning of downstroke, the steep separation is weakened slightly while a reduction in lift hysteresis from 21° down to 11° and the advance of reattachment angle can be observed on downstroke with plasma actuation. Among the three actuation frequencies, $F^+ = 1$ and $F^+ = 2$ have better flow control effect in the lift enhancement on downstroke but the effect for earlier reattachment is almost the same. The attachment angle with NS-DBD actuation is 2 degrees earlier than baseline curve. In terms of the area of the hysteresis loop, the maximum reduction of the area (38.3%) is achieved at $F^+ = 1$, while the reduction of 36.4% and 29.6% are also achieved at $F^+ = 2$ and $F^+ = 3$ respectively.

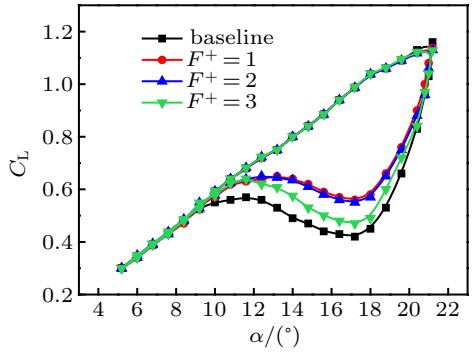

Fig. 8. Flow control effects under light stall state ($k = 0.05$).

3.2.2. Flow control effects at $k = 0.1$

Figure 9 shows the flow control results of light stall state at $k = 0.1$. The control effect occurs at almost the same range of angle of attack as $k = 0.5$. With plasma on, the lift coefficient changes little on upstroke. At this time, the lift coefficient is not increased and the stall angle is not delayed; On downstroke, the steep decrease of lift coefficient is alleviated and the recovery of lift coefficient is relatively faster. From 20° to 11° of downstroke, the lift coefficient is significantly promoted for all actuation frequencies, resulting in earlier reattachment and the reduction of the area of the hysteresis loop. The area is reduced by 20.8% at $F^+ = 1$ and the reduction 19.8% and 15.6% are achived at $F^+ = 2$ and $F^+ = 3$, respectively.

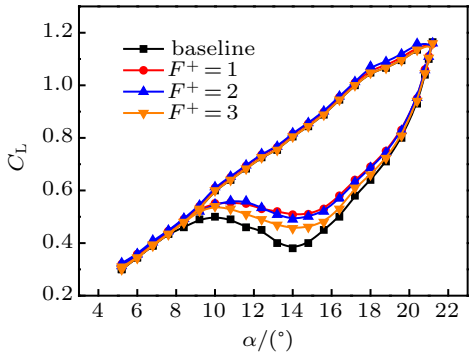

Fig. 9. Flow control effects under light stall state ($k = 0.1$).

3.2.3. Flow control effects at $k = 0.15$

Compared with cases at $k = 0.05$ and $k = 0.1$ introduced above, the flow control effect at $k = 0.15$ is relatively much weaker with the same actuation conditions, as shown in Fig. 10. Only in the range of angle of attack from 17° to 13°

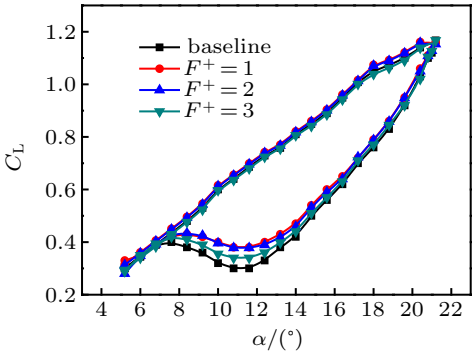

Fig. 10. Flow control effects under light stall state ($k = 0.15$).

on downstroke, the small increase in the lift coefficient can be observed. Moreover, the attachment angle has not been advanced in this condition. The area of the hysteresis loop is reduced by 16.8% at $F^+ = 1$ and $F^+ = 2$ and it is reduced by 8.9% at $F^+ = 3$.

3.3. Flow control of deep stall state

With the same set of flow conditions and actuation parameters, wind tunnel tests were conducted under deep dynamic stall state with a motion profile of $\alpha = 14.85 + 9.45 \times \sin(\omega t)$ for various reduced frequencies ($k = 0.05$, $k = 0.1$, and $k = 0.15$). Naturally, the range of α was 5.4°–24.3°. Before flow control experiments, the baseline lift coefficients for various reduced frequencies were also investigated. The results are shown in Fig. 11. When the airfoil pitches up to $\alpha = 21°$ prior to the maximum angle of attack, the lift begins to drop and the stall occurs. At the beginning of the downstroke proccess, the lift coefficient does not stop dropping until it reaches the the minimum value of upstroke process, this value is even smaller than the minimum value at $k = 0.15$. As the airfoil continues pitching down, the boundary layer begins to attach and lift coefficient rises up slowly. It is worth note that when $k = 0.05$ and $k = 0.1$, the recovery of lift coefficient can be observed. But when $k = 0.15$, only subtle recovery of lift can be observed, which can even be ignored. However, the variation of baseline with increased reduced frequency is similar to that of light stall. Similar to the arrangement of light stall experiments, various dimensionless actuation frequencies were used in the flow control test to determine the NS-DBD's control capabilities under deep dynamic stall state.

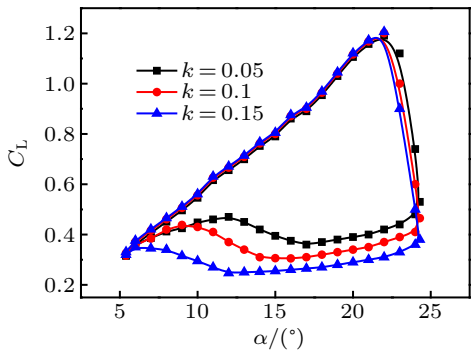

Fig. 11. Baseline for various reduced frequencies of deep dynamic stall.

3.3.1. Flow control effects at $k = 0.05$

For deep dynamic stall cases, the flow control results at various dimensionless actuation frequencies at $k = 0.05$ are shown in Fig. 12. The hysteresis effect is more severe under deep stall and the flow control effect is not as obvious as that in light stall condition. Similarly, NS-DBD does not achieve flow control effect on upstroke and at the stage of high α. The NS-DBD starts to gain benefits when the airfoil begins to pitch down. The improvement of lift coefficient and earlier reattachment can be observed from 23° down to 8° on downstroke and the attachment angle of attack with NS-DBD actuation is 2° earlier than baseline for all actuation states. In comparison, the control effect at $F^+ = 1$ is the best, while $F^+ = 2$ is the second, and $F^+ = 3$ is the worst. At $F^+ = 1$, the area of the hysteresis loop is reduced by 13.2%, while at $F^+ = 2$, it is reduced by 12.8%. At $F^+ = 3$, the corresponding value is only about 9.6%.

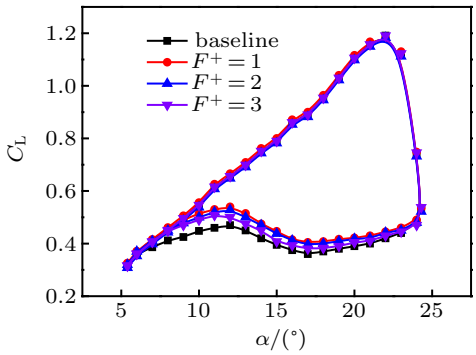

Fig. 12. Flow control effects under deep stall state ($k = 0.05$).

3.3.2. Flow control effects at $k = 0.1$

At $k = 0.1$, the flow control effect is shown in Fig. 13. It is obvious that there is no control effect on the whole of upstroke and at the beginning of downstroke.When the airfoil pitches down to 22°, the lift coefficient is increased and the lift recovery is advanced under all actuation states. The attachment angle of attack at $F^+ = 1$ and $F^+ = 2$ is 1° earlier than the baseline. In terms of the area of the hysteresis loop, it can be reduced by 12.6%, 10.8% and 8.9% at $F^+ = 1$, $F^+ = 2$, and $F^+ = 3$, respectively.

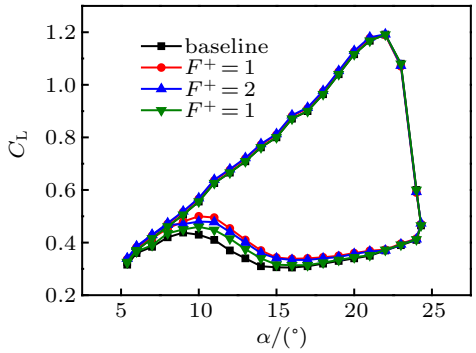

Fig. 13. Flow control effects under deep stall state ($k = 0.1$).

3.3.3. Flow control effects at $k = 0.15$

When $k = 0.15$, based on the baseline results, the stall is so severe that lift is difficult to recover. Under the actuation conditions set in this paper, the flow control effect is very weak compared to other reduced frequencies states, as shown in Fig. 14. The actuation is not effective until the airfoil pitches down to 13°. The improvement of lift coefficient at the stage of small α on downstroke is insignificant. It is as if the NS-DBD actuation suddenly does not work. The area of the hysteresis loop is reduced by no more than 4% under all actuation

states. This indicates the difficulty of deep dynamic stall control at large reduced frequencies, although the flow separation is reduced at lager k.

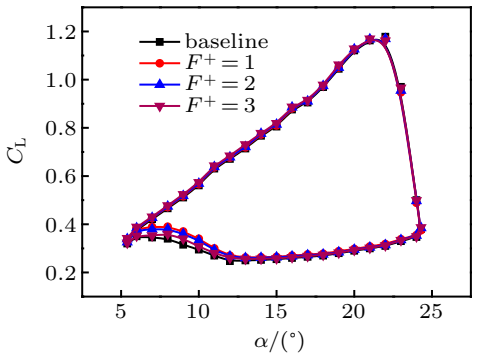

Fig. 14. Flow control effects under deep stall state ($k=0.15$).

From the overall trend of lift coefficients in all experimental states, it can be seen that, no flow control effect can be achieved by NS-DBD on upstroke no matter in whether it is light stall state or deep stall state. The increase of lift can be observed around the maximum angle of attack but the stall angle can not be delayed. However, the lift coefficient can be increased within certain α on downstroke with plasma actuation. The effective range of α for NS-DBD flow control decreases with the increase of k. On the whole, the NS-DBD actuation could play a certain role in controlling the DSV formed by the airfoil motion so the area of hysteresis loop could be reduced and the sharp separation could be eased. Compared with the deep stall state, the flow control effect under the light stall state is more obvious, with C_L corresponding to each k recovering faster and the reattachment angle appearing earlier. The lift coefficient at large α can also be improved under the light stall state. For the same stall state, the control effect gets worse with the increase of k. The mechanism of these phenomenons are disccussed in the next section.

4. Analysis of experimental results and flow control mechanism

4.1. Mechanism of airfoil flow separation control by NS-DBD

With the experimental results above, it is found that the dynamic stall control is quite different from that of the static case. The effect of delaying the stall angle and enhancing the peak lift coefficient like that in static flow separation control has not been observed. According to the existing principles on airfoil stall control in static cases by NS-DBD plasma actuation,[28,29] when the flow separation occurs over the airfoil at high α, the NS-DBD actuation employed at the leading edge can induce a strong span-wise vortex at the leading edge shear layer, accompanied with the induced shock wave propagating outward rapidly. The span-wise vortex is attached to the airfoil, keeps growing and moving downstream. In the process, these vortices gain energy and momentum from the shear layer, and promote the momentum mixture between freestream and the boundary layer, which causes the suppression of flow separation and the enhancement of the lift coefficient and stall angle. The evolution of flow fields with and without NS-DBD actuation in Ref. [30] is shown in Fig. 15.

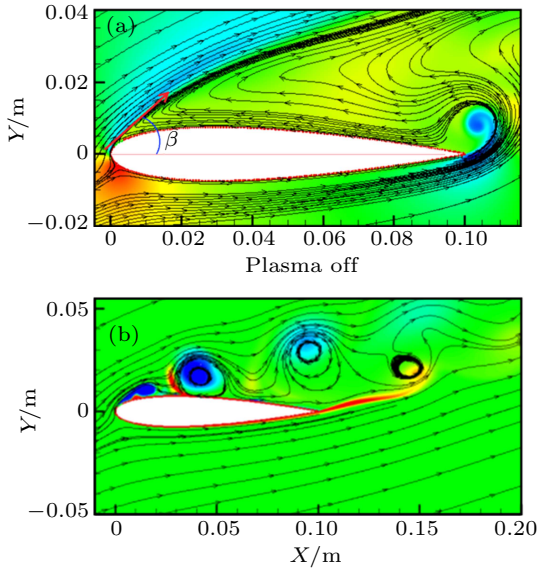

Fig. 15. Flow field over a static airfoil with and without NS-DBD:[30] (a) plasma off and (b) plasma on.

In general, the NS-DBD actuation can delay the airfoil's stall angle by 2°–5° at low-speed flow conditions for different airfoils. When α increases to a certain level, the separation control becomes difficult. This is not only due to the limitation of actuation intensity of NS-DBD, but also due to the enhanced deflected angle of the separated shear layer at large angle of attack. The deflected angle of the separated shear layer β can be defined as the angle between the leading-edge separated shear layer and the airfoil chord, as shown in Fig. 15(a). The large β causes large adverse pressure gradient, making the span-wise vortex move along the shear layer. Because of this, the vortex is difficult to be locked on the airfoil's upper surface. Ultimately, the induced span-wise vortex is merged into the large scale separation region. In this case, the separation is difficult to control.

4.2. Discussion of flow control effects at the effective range of α

From the experimental results of all actuation states, it is found that for a fixed reduced frequency k, the NS-DBD actuation could not delay the stall angle, and the control effect at the high α is limited. When the airfoil pitches up to the stage of high α, due to the action of the down-wash stream and the dynamic stall vortex, the dynamic stall angle is much larger than that of the static case,[31] and the corresponding maximum lift coefficient is also higher than that of the static airfoil. However, once the dynamic stall vortex separates from the airfoil's upper surface, dynamic stall occurs. At this moment,

both α and β are large enough to produce severe adverse pressure gradient. This may exceed the flow control ability of the NS-DBD actuation. The schematic diagrams of the flow field under baseline and actuation states are shown in Figs. 16(a) and 16(b). Even if the span-wise vortex is produced by the NS-DBD, the vortex will be swallowed by the stronger separated region, making the separation unable to be effectively controlled. In this condition, the momentum mixture promoted by the plasma actuation between the freestream and boundary layer is limited, which is insufficient to change the stall state.

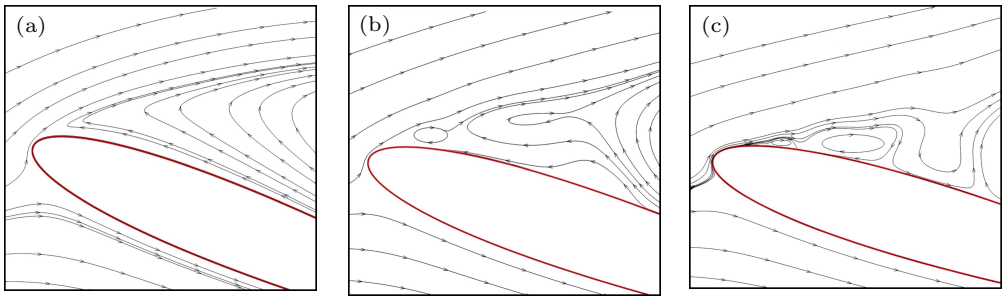

Fig. 16. Flow field with and without actuation for dynamic stall: (a) base flow field at high α, (b) flow field with actuation at high α, (c) flow field with actuation when airfoil pitching down to a certain degree.

As shown in Fig. 16(b), when the airfoil starts pitching down from the maximum α, the up-wash flow becomes obvious gradually and the effective α becomes larger. Coupled with the large β, this leads to the severe adverse pressure gradient, causing the serious flow separation. However, it is difficult for NS-DBD to resist the adverse pressure gradient in this condition.

Only when the effective α decreases to a certain degree and the β becomes small enough will the adverse pressure gradient be moderated. Here, the phenomenon that the flow control effect only occurs during the pitching-down phase is consistent with Refs. [32,33]. Then, the plasma actuation can induce a closed span-wise vortex being able to be locked on the airfoil, similar to the effective flow control of static separation, as shown in Fig. 16(c). In this condition, NS-DBD can play an effective role in the flow separation control, which can be seen in the rapid recovery of lift and early reattachment of airflow on downstroke. The macroscopic control result and the effect difference of different dimensionless actuation frequencies can be analyzed from the microscopic flow field. Briefly, the formation of airfoil-closed span-wise vortex (coherent structures) induced by NS-DBD actuation entrains high-momentum flow from the freestream and results in momentary reattachment.[23,24] However, the coherent structures induced by different dimensionless frequencies are different. At low dimensionless actuation frequencies (usually $F^+ < 2$), the induced structures are large, which can result in an earlier attachment Angle and airflow attachment at a greater range of α. The formation of small structures (such as those produced by higher dimensionless actuation frequencies) only results in partial reattachment.[23,24] Earlier flow reattachment reduces the aerodynamic hysteresis. This results in the least decrease of hysteresis loop area under $F^+ = 3$ actuation.

Therefore, the flow control effect for dynamic stall is mightily dependent on the history of angle of attack.

4.3. Effect of reduced frequency on dynamic stall control

Reduced frequency is used to describe the flow instability of airfoil or wing. Wang *et al.*[34] point out that reduced frequency value greater than 0.05 is more critical. Unstable aerodynamics will lead to large fluctuations of airfoil surface pressure, which will increase the load. Therefore, flows can be considered quasi-steady if $k < 0.05$. Zhao[35] has carried out numerical simulation for typical airfoil conditions ($k = 0.05$, $k = 0.1$, and $k = 0.15$) respectively, and finds that with the increase of reduced frequency, the hysteresis effect of aerodynamic coefficient is more intense and the area of hysteresis loop increased, which is consistent with the experimental results in this paper. At the same time, the peak of the nose-down moment increases with the increase of the reduced frequency and moves back. Zhang *et al.*[36] also reach the same conclusion. On the one hand, during the increase of α, the hysteresis effect of the separation point is more significant. On the other hand, the lift recovery delay is more significant on downstroke, and the lift coefficient decreases more.

In general, the reduced frequency represents the strength of the dynamic stall characteristic of the airfoil. The greater the reduced frequency is, the stronger the dynamic characteristic and hysteresis effect will be, and conversely, the weaker the dynamic characteristic will be. This conclusion can be understood from the perspective of the airfoil oscillation motion. On upstroke, the larger k is, the more obvious the induced leading edge downwash effect is, making the airfoil effective α smaller, and leading edge is difficult to separate. While with the increase of k on downstroke, the induced upwash effect on the leading edge becomes more obvious, which makes the airfoil effective α lager, leading edge easier to separate, and the recovery of lift slower. Therefore, the dynamic hysteresis effect becomes more obvious. From the perspective of the variation of aerodynamic hysteresis characteristics and nose-down moment, the larger k is, the more difficult it is to control

the dynamic stall once it occurs.

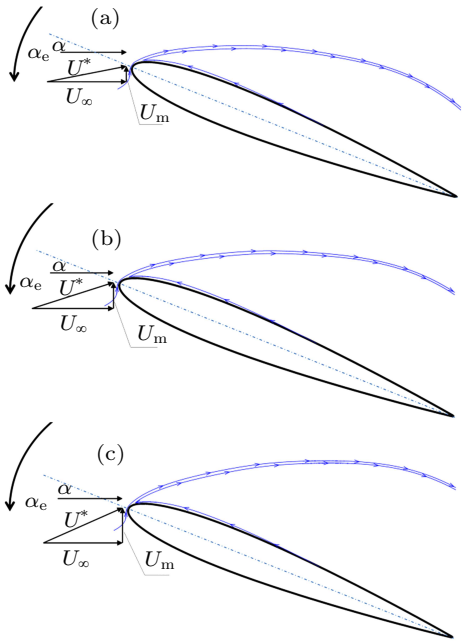

Fig. 17. Analysis for effect of various k at certain α on downstroke: (a) $k = 0.05$ pitch-down motion, (b) $k = 0.1$ pitch-down motion, and (c) $k = 0.15$ pitch-down motion.

In this paper, whether in light stall state or in deep stall state, the flow control effect becomes worse with the increase of k and the effective flow control only occurs at partial range of α on downstroke. As shown in Fig. 17, for the same freestream velocity U_∞, mean angle of attack α_0 and motion amplitude α_m, larger k means greater change rate of α ($\alpha_m \omega \cos(\omega t)$). When the airfoil pitches down to certain α, the up-wash velocity U_m induced by the oscillation motion is also larger for cases with larger k, leading to a larger combined velocity U^* which is the vector sum of U_m and U_∞. Hence, the effective angle of attack α_e of airfoil becomes larger and the deflected angle of the separated shear layer β is larger too. The corresponding separation region will expand and the separation will be more difficult to control. Therefore, at a large reduced frequency ($k = 0.15$), the control effect is obtained only at smaller α on downstroke. Conversely, when k is small, the up-wash velocity (U_m) induced by the oscillation motion is small so that the deflected angle of the separated shear layer β is relatively small. The perturbation induced by NS-DBD actuation can promote the exchange of the energy and momentum on both sides of the shear layer effectively, which is beneficial to the formation and development of the attached span-wise vortex. Therefore, better lift recovery and wider range of α with flow control effect can be observed at $k = 0.05$ and $k = 0.1$.

4.4. Analysis of results under different dynamic stall states

The stall state is determined by the mean angle of attack α_0 and motion amplitude α_m. The α_0 and α_m of deep stall are larger than those of light stall. Wang[37] have studied the influence of α_0 and α_m on airfoil dynamic stall characteristics, and finds that α could effectively affect the adverse pressure gradient near the leading edge. With the increase of α_0, the airfoil dynamic stall characteristics are aggravated. Under high α_0, the stall is more intense, the hysteresis loop area is larger, and the strength of the leading edge separation vortex is larger. With the increase of α_m, the dynamic stall characteristic of the airfoil is also enhanced, that is, it has a larger stall α, a higher peak of lift coefficient, and a smaller reattachment α. Therefore, the area of hysteresis loop also increases with the increase of α_m. Under high α_m, the peak moment coefficient is higher, which is mainly because the leading edge separation vortex under high α_m is stronger, so the induced nose-down moment when it moves to the trailing edge of the airfoil is also larger.

In conclusion, the dynamic hysteresis effect of deep stall state is more intense, so the stall is more difficult to control. Therefore, under the actuation parameter combination set in this paper, different results for various reduced frequencies under the light stall state and deep stall state appear. Relatively speaking, the greater k is, the worse the control effect is and overall control results under deep stall state are not as good as those under light stall state.

5. Conclusion

In view of the outstanding ability and advantages of NS-DBD in flow separation control for subsonic flows, the dynamic stall control experiments based on NS-DBD actuation were conducted on an NACA 0012 airfoil in wind tunnel. The flow control effects were investigated and the influence law of reduced frequency and dimensionless actuation frequency were explored by direct force measurement under light and deep dynamic stall conditions. Based on the experimental results, the mechanism of the dynamic stall control by NS-DBD actuation was analyzed and discussed. Major conclusions are as follows:

(i) For the stall characteristics of the static airfoil, the lift of the airfoil is significantly improved by the NS-DBD actuation, and the stall angle is delayed by about 4°.

(ii) For both light and deep dynamic stall states, the dynamic stall angle is not delayed and the stall state does not changed with actuation.

(iii) On upstroke, no flow control effect is acquired. When the airfoil pitches into downstroke, the lift coefficient can be promoted for all actuation frequencies, resulting in faster lift recovery, earlier reattachment and the reduction of the area of the hysteresis loop. Among three dimensionless actuation frequencies, $F^+ = 1$ is the best. The steep decrease of lift coefficient can be alleviated under light dynamic stall. The control effect of the light stall state is better than that of deep stall state.

(iv) The reduced frequency has a great influence on the dynamic stall control. As the reduced frequency increases, the flow control effect gets weaker. The larger the reduced frequency is, the more difficult it is to control and improve the dynamic stall.

(v) Different from static separation control, the dynamic stall has a larger separation angle of leading-edge shear layer, which is difficult to be controlled at large angles of attack. Only when the angle of attack is decreased to a certain extent can the flow control effect be achieved, especially with larger reduced frequency. Therefore, the dynamic stall control is greatly affected by the reduced frequency, and the flow control effect of dynamic stall is strongly dependent on the history of angle of attack.

References

[1] Xing S L, Xu H Y, Ye Z Y, Ma M S and Xu Y 2020 *Int. J. Mod. Phys. B* **34** 2040108
[2] Raghav V and Komerath N 2014 *Experiments in Fluids* **55** 1669
[3] Wang R and Xia P Q 2013 *Sci. China Technol. Sci.* **1** 175
[4] Wen G and Gross A 2019 *AIAA J.* **57** 1434
[5] Visbal M R and Benton S I 2018 *AIAA J.* **56** 2974
[6] Ye Z L, Wang X D, Chen Z W and Wang L Y 2020 *Acta Mech. Sin.* **36** 320
[7] Fu L, Yang C, Zhang H and Bao W R 2020 *Proceedings of the Institution of Mechanical Engineers Part D Journal of Automobile Engineering* 095440702091656
[8] Veerakumar R, Raul V, Liu Y, Wang X D, Leifsson L and Hu H 2020 *Acta Mech. Sin.* **36** 260
[9] Messanelli F, Frigerio E, Tescaroli E and Belan M 2019 *Experimental Thermal & Fluid Science* **105** 123
[10] Walker S and Segawa T 2012 *Renewable Energy* **42** 105
[11] Henne S, Parikh A, Deparday J and Mulleners K 2018 *International Symposium on the Applications of Laser & Imaging Techniques to Fluid Mechanics*
[12] Post M L and Corke T C 2006 *AIAA Journal* **44** 3125
[13] Jiang J, Yang A M and Weng P F 2008 *Journal of Shanghai University (Natural Science)* **14** 405
[14] Mai H, Dietz G, Geissler W and Richter K 2008 *Journal of the American Helicopter Society* **53** 26
[15] Ben-Harav A and Greenblatt D 2016 *Wind Energy* **19** 3
[16] Castañeda D, Whiting N, Webb N J and Samimy M 2019 *AIAA Aviation 2019 Forum* 3212
[17] Rethmel C, Little J, Takashima K and Sinha A 2011 *Int. J. Flow Control* **3** 213
[18] Cattafesta L N and Sheplak M 2011 *Ann. Rev. Fluid Mech.* **43** 247
[19] Corke T C, Enloe C L and Wilkinson S P 2010 *Ann. Rev. Fluid Mech.* **42** 505
[20] Wang J J, Choi K S, Feng L H, Timothy N J and Whalley R D 2013 *Progress in Aerospace Sciences* **62** 52
[21] Roupassov D, Zavialov I and Starikovskii A 2006 44*th AIAA Aerospace Sciences Meeting and Exhibit*, AIAA-2006-373
[22] Frankhouser M, Hird K, Naigle S, Gregory J W and Bons J P 2015 46*th AIAA Plasmadynamics and Lasers Conference*, American Institute of Aeronautics and Astronautics
[23] Starikovskiy A, Meehan K and Miles R B 2018 *AIAA Aerospace Sciences Meeting* 0681
[24] Singhal A, Castañeda D, Webb N J and Samimy M 2018 *AIAA Journal* **56** 78
[25] Chen W X 2008 *Helicopter Technique* **155** 4
[26] Mulleners K and Raffel M 2012 *Experiments in Fluids* **52** 779
[27] Chandrasekhara M and Carr L 1995 *AGARD FDP Symposium* CP-552
[28] Chen Z L, Hao L Z and Zhang B Q 2013 *Sci. China-Series A-Math. Phys. Astron. & Technol. Sci.* **56** 1055
[29] Ullmer D, Peschke P, Terzis A and Ott P 2015 *J. Phys. D: Appl. Phys.* **48** 365203
[30] Zhao G Y, Li Y H, Liang H, Hua W Z and Han M H 2015 *Acta Phys. Sin.* **64** 015101 (in Chinese)
[31] Wei B, Wu Y, Liang H, Su Z and Li Y H 2019 *Aerospace Science and Technology* **96** 105584
[32] Mitsuo K, Watanabe S, Atobe T and Kato H 2013 *AIAA Aerospace Sciences Meeting Including the New Horizons Forum & Aerospace Exposition*
[33] Fukumoto H, Aono H, Nonomura T and Oyama A 2016 *AIAA Flow Control Conference*
[34] Wang F and Cui J Q 2015 *Flight dynamics modeling of coaxial rotorcraft UAVs* (Berlin: Springer) pp. 1217–1256
[35] Zhao G Q 2015 *CFD Simulation of unsteady dynamic stall of helicopter rotor and active flow control* (Nanjing: Nanjing University of Aeronautics and Astronautics) pp. 58–63 (in Chinese)
[36] Zhang R M, Zhao J B and Guo S J 2016 *Aeronautical Computing Technique* **46** 75
[37] Wang Q 2017 *Research on dynamic stall mechanics mechanism and aerodynamic shape optimization of rotor* (Nanjing: Nanjing University of Aeronautics and Astronautics) pp. 61–72 (in Chinese)